Dinh *et al. Int J Concr Struct Mater* (2025) 19:16
https://doi.org/10.1186/s40069-024-00754-0

International Journal of Concrete Structures and Materials

RESEARCH **Open Access**

Modification of KDS 14 Design Model for Punching Shear Strength of Slab–Column Connections Reinforced with Various Types of FRP Rebars

Ngoc Hieu Dinh[1], Si-Hyun Kim[1] and Kyoung-Kyu Choi[1*]

Abstract

The current Korean Standard KDS 14 has adopted a strain-based shear strength model for evaluating the punching shear strength of slab–column connections reinforced with steel rebars. Thus, this study evaluated the applicability of the KDS 14 design model for slab–column connections reinforced with FRP rebars. The KDS 14 model was improved by modifying the equation for determining the depth of the compression zone, taking into account the material characteristics of FRP reinforcement. The modified KDS 14 model was evaluated by conducting a comparative analysis with existing design codes over a comprehensive database of 150 interior FRP-reinforced interior slab–column specimens with and without shear reinforcement. The results indicated that the modified KDS 14 model provided promising performance over various design parameters by exhibiting a similar scatter and conservatism compared to the JSCE 2007 and CSA codes with a COV of approximately 15%, while showing better correlation with the dataset than most existing design codes. In addition, a parametric analysis was conducted to investigate the primary design parameters that affected the punching shear stress capacity at the critical section of FRP-reinforced slab–column connections using both the modified KDS 14 model and existing design codes. Overall, all prediction models exhibited similar trends. Further, they were consistent with the experimental results according to variations in design parameters, including concrete compressive strength, slab effective depth, FRP axial stiffness, and column dimension.

Keywords Punching shear, Shear stress, Analytical model, Fiber-reinforced polymer, Compression zone, KDS 14 design code

1 Introduction

In recent years, climate change and global warming, which cause biodiversity loss and pose a threat to the natural environment, have garnered significant global attention. Human activities are considered a critical contributing factor to these issues (Pavlović et al., 2022). In the construction industry, building material production (e.g., cement, steel, and aluminum) has been found to cause a considerable amount of carbon emission, accounting for over 10% of global carbon emissions (Watari et al., 2022). Thus, the concept of sustainability in construction has been introduced to assess the negative impacts of construction materials on the environment. In terms of reducing carbon emissions, the construction materials that produce less carbon are considered more sustainable. In addition, the corrosion of steel rebars is a severe issue that shortens the durability and the service life of RC structures. Over the past decades,

*Correspondence:
Kyoung-Kyu Choi
kkchoi@ssu.ac.kr
[1] School of Architecture, Soongsil University, 369 Sangdo-Ro, Dongjak-Gu, Seoul 153-743, South Korea

fiber-reinforced polymer (FRP) bars have emerged as an eco-friendly alternative to steel rebars in structural systems in practical projects. They can aid in the achieving the goals of net-zero carbon emissions and improved durability (Ray et al., 2015; Watari et al., 2022). FRP rebars offer several advantages compared to steel bars, such as resistance to corrosive and alkaline environments, high strength-to-weight ratio, and a significantly lower carbon footprint during the production process. These characteristics address both sustainability and durability concerns while ensuring reliable mechanical performance owing to their high tensile strength.

The flat slabs are integral components in the construction of modern buildings. They offer versatile and efficient structural solutions for various architectural designs. The structural integrity and longevity of flat slabs are paramount in their design and construction, particularly in high-rise buildings and structures that are subjected to heavy loads and harsh environmental conditions. This has resulted in the widespread application of FRP bars in flat plate systems (Mohamed & Khattab, 2017). However, design and performance of flat-plate systems are affected by the punching shear failure at slab–column connections. Figure 1 illustrates the typical punching shear failure and critical section at slab–column connections in a flat-plate system. Such failures occur when the shear stress developed under applied load surpasses the shear capacity of the slab around the column, leading to a sudden and brittle failure with an apparent punching cone (Dinh et al., 2024a). This causes considerable damage or even structural collapse. The mechanisms governing punching shear failure are complex and influenced by various factors, including the characteristics of the concrete, the mechanical performance of the reinforcing materials, and the bond behavior between the reinforcing bars and surrounding concrete (Dinh et al., 2024b). Owing to differences in mechanical and physical properties, the punching shear behavior of FRP-reinforced concrete (FRP-RC) flat plates is different from that of conventional steel-reinforced concrete (steel-RC) flat plates (Almomani et al., 2024; Dinh et al., 2024c). Steel exhibits elastoplastic behavior, whereas FRP materials remain linear in the elastic range until failure. In addition, the elastic modulus of FRP is lower than that of steel (approximately 1/4–1/2 of the steel modulus). These differences necessitate the careful consideration of the punching shear capacity within the design of FRP-RC flat plate systems.

Various experimental investigations have been conducted to understand the design parameters that influence the punching shear behavior of FRP-RC flat slabs. These studies are the basis for the current design formulations. Matthys and Taerwe (2000) investigated 17 concrete slabs reinforced with different types of FRP rebars under concentric loading. They found that FRP-RC slabs exhibited punching shear resistance similar to that of steel-RC slabs for the same flexural stiffness. El-Ghandour et al. (2003) and Ospina et al. (2003) reported that the punching shear capacity of FRP-RC slabs was influenced by the flexural stiffness of the FRP rebars and the bond performance between the FRP reinforcement and surrounding concrete. Lee et al. (2009) showed that the punching shear performance of glass FRP-RC slabs could be improved by concentrating the reinforcement within a distance of 1.5 times the slab thickness from the column edges. Further, Dulude et al. (2013) and Hassan et al. (2013b) demonstrated that the punching shear capacity of FRP-RC slabs increased with greater slab thickness, larger column size, and higher concrete strength.

In terms of practical design, various empirical and semi-empirical approaches have been adopted for evaluating the punching shear strength of two-way

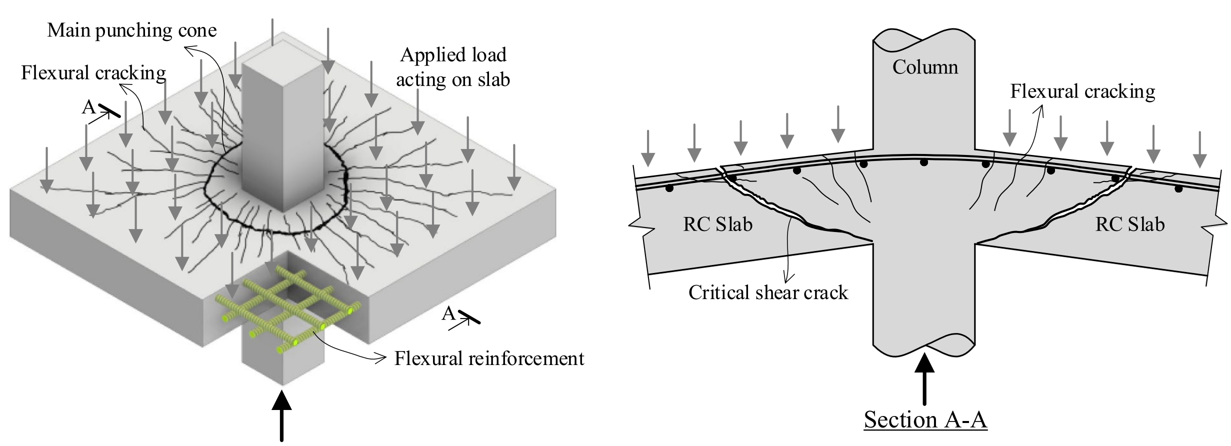

Fig. 1 Punching shear failure and critical section at slab–column connections

Table 1 Summary of punching strength models for FRP-RC slab–column connections

Models	Shear strength equations
ACI 440.1R-15 (2015)	$V_c = \frac{4}{5}\sqrt{f'_c}b_0kd$ $k = \sqrt{2\rho_f n_f + (\rho_f n_f)^2} - \rho_f n_f, n_f = E_f/E_c$
ACI 440.11–22 (2022)	$V_c = 0.83\lambda_s k_{cr}\sqrt{f'_c}b_0d \geq V_{c,\min}$ $k_{cr} = \sqrt{2\rho_f n_f + (\rho_f n_f)^2} - \rho_f n_f, \lambda_s = \sqrt{2/(1+0.004d)} \leq 1.0, V_{c,\min} = 0.13\lambda_s\sqrt{f'_c}b_0d$
JSCE (2007)	$V_c = \beta_d\beta_p\beta_r\frac{f_{pcd}}{\gamma_b}\frac{1}{\alpha_e}b_0d$ $\beta_d = \sqrt[4]{1000/d} \leq 1.5(d \text{ in mm}), \beta_p = \left(100\rho_f\frac{E_f}{E_s}\right)^{1/3} \leq 1.5, \beta_r = 1 + 1/(1+0.25u_0/d)$ $f_{pcd} = 0.2\left(f'_c\right)^{0.5} \leq 1.2\,\text{MPa}, \alpha_e = 1 + 1.5\left[(e_x+e_y)\sqrt{b_xb_y}\right]$
CSA/S806-12 (2021)	The smallest of the following values: $V_c = 0.028\lambda_s\lambda\phi_c\left(1+\frac{2}{\beta_c}\right)\left(E_f\rho_f f'_c\right)^{1/3}b_0d$ $V_c = 0.147\lambda_s\lambda\phi_c\left(\frac{\alpha_s d}{b_0}+0.19\right)\left(E_f\rho_f f'_c\right)^{1/3}b_0d$ $V_c = 0.056\lambda_s\lambda\phi_c\left(E_f\rho_f f'_c\right)^{1/3}b_0d$ $\lambda_s = 1 \text{ for } d \leq 300, = (300/d)^{0.25} \text{ for } d > 300$
Modified KDS 14 model	$V_c = k_sk_{b0}c_ub_0\sqrt{f_{te}(f_{te}+f_{cc})}$ $f_{te} = 0.2\sqrt{f'_c}, f_{cc} = 2/3f'_c, k_s = 0.75 \leq \sqrt[4]{300/d} \leq 1.1(d \text{ is in mm}), k_{b0} = 4/(\alpha_s b_0 d)^{0.5} \leq 1.25,$ $c_u = d\left(25\sqrt{\frac{\rho_{s,e}}{f'_c}} - 300\frac{\rho_{s,e}}{f'_c}\right), \rho_{s,e} = \rho_f\frac{E_f}{E_s}$

f'_c = concrete compressive strength; b_0 = critical perimeter at a distance of 0.5d from the column face; d = effective depth of slab; ρ_f = FRP reinforcement ratio; E_f, E_s, and E_c = elastic modulus of FRP, steel, and concrete, respectively; k (k_{cr}) = factor to account for the neutral axis depth; n_f = modulus ratio; λ_s, k_s, and β_d = size effect factor; β_p = factor to account for axial stiffness of FRP reinforcement; β_r = factor to account for column perimeter-to-depth ratio; β_c = the ratio of the long side to the short side of the column cross-section; u_0 = column perimeter; γ_b [= 1.3] = safety factor; α_e = factor to account for load eccentricity; λ = factor to account for concrete density; φ_c = resistance factor for concrete; f_{te} = effective tensile strength of the concrete; f_{cc} = average compressive stress in compression zone; k_{b0} = aspect ratio factor of the critical section; α_s = factor to account for the location of the connections, α_s is set to 1, 1.33, and 2 for interior, exterior, and corner connections, respectively; and c_u = depth of the compression zone slabs reinforced with FRP reinforcement. Table 1 summarizes the evaluation equations of different design codes. The ACI 440.1R-15 (2015) model can determine the concrete contribution (V_c) to the direct punching shear resistance of FRP-reinforced slab–column connections within the critical section perimeter at a distance of 0.5 times the slab effective depth (d) from the column faces. This model is based on the modifications of the ACI 318-14 (2014) method for steel-reinforced concrete slabs by considering parameters such as the longitudinal FRP reinforcement ratio (ρ_f), square root of concrete compressive strength ($f'^{0.5}_c$), and modulus ratio between FRP reinforcement and concrete. Previous studies have reported that the ACI 440.1R-15 (2015) model provided overly conservative predictions compared to experimental results (Peng et al., 2020). In the recent ACI 440.11-22 (2022), the prediction model used a similar shear approach to that of ACI 440.1R-15 but incorporated modifications to consider the member depth size effect (λ_s) and the minimum shear strength of the concrete contribution. The JSCE (2007) directly considers the axial stiffness of FRP rebars ($\rho_f E_f$), size effect, the column perimeter-to-effective depth ratio (u_0/d), and the loading eccentricity. The design method used in the CSA S806-12 code (2021) is based on the concept of shear force limitation resisted along the defined 45° failure surface. Further, the concrete contribution is considered as proportional to the square root of the concrete compressive strength. In addition, the CSA code also considers the reduced concrete strength owing to the concrete resistance factor ϕ_c [=0.65] and the critical section perimeter at a distance of $d/2$ from the column faces, similar to the ACI and JSCE codes. Recently, the Korean Standard KDS 14 20 22 (2021) adopted the strain-based shear strength model theoretically developed by Choi et al. (2014) for evaluating the direct punching shear capacities of steel-RC slab–column connections. This model has exhibited a strong correlation with test results from a comprehensive database (Choi & Park, 2010). Consequently, the prediction model based on KDS 14 should be modified and assessed to be applicable to the design of FRP-reinforced concrete (FRP-RC) members.

To address this limitation, this study introduced modifications to the existing KDS 14 design model for predicting the punching shear strength of slab–column connections reinforced with FRP rebars, specifically accounting for the material properties of FRP flexural reinforcement. The reliability of the modified KDS 14 model was evaluated through rigorous comparisons using a comprehensive experimental dataset that contained specimens with and without shear reinforcement. Moreover, the predictive performance of the modified KDS 14 model was compared with that of the existing state-of-the-art design codes. In addition, a detailed parametric analysis was conducted to investigate the

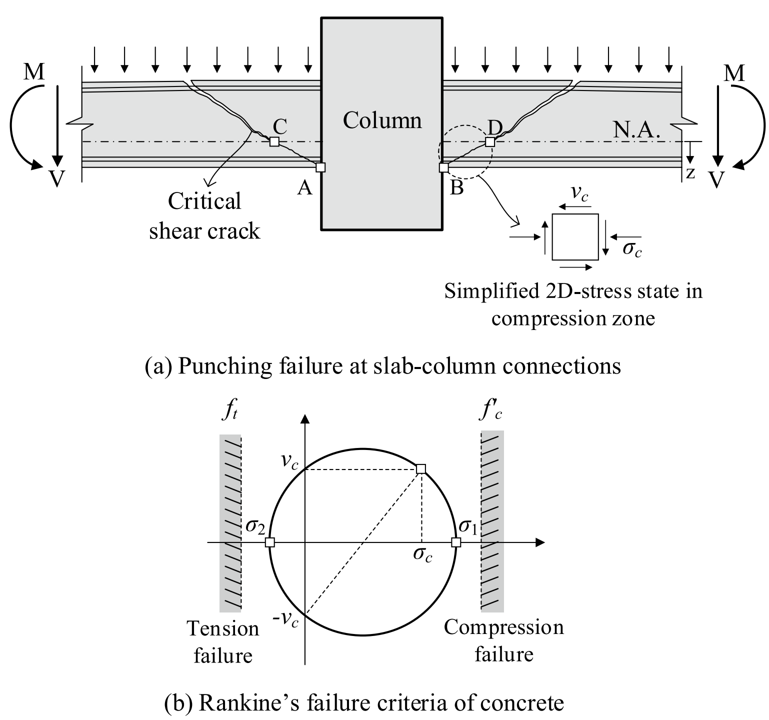

Fig. 2 Stress state and failure criteria of concrete at the critical section of slab–column connections

influence of key parameters on the punching shear strength of FRP-RC slab–column connections.

2 Review of Punching Capacity of Slab–Column Connections Based on Compression Zone Failure Mechanism

In the KDS 14 design method, the punching shear strength of slab–column connections is determined based on the theoretical background of compression zone failure mechanisms developed by Choi et al. (2014). As shown in Fig. 1, the punching failure of slab–column connections reinforced with FRP rebars or steel rebars typically occurred following the formation of significant flexural cracking, similar to the behavior observed in slender beams (Dulude et al., 2013; El-Ghandour et al., 2003; Lee et al., 2009; Schmidt et al., 2020). Consequently, the shear strength of RC slab–column connections can be determined considering the shear resistance capacity of the intact concrete in the compression zone. Figure 2 shows the stress state at the critical section around the connection, wherein the concrete was subjected to a combination of compressive and shear stresses induced by the slab's flexural and shear actions. In the KDS 14 model, the average shear stress capacity, v_c, in the compression zone is determined using the average compressive stress, f_{cc}, of the compression zone using Rankine failure criteria (Choi et al., 2014) (Fig. 2b):

$$v_c = \int_0^{c_u} v_{nt}(z)dz/d \approx \sqrt{f_{te}(f_{te}+f_{cc})}c_u/d \tag{1}$$

where v_{nt} is the shear-stress capacity controlled by tension, $f_{te}\left[=0.2\sqrt{f_c'}\right]$ is the effective tensile fracture strength of concrete, f_c' is the compressive strength of concrete, d is the effective depth of slab, and c_u is the depth of compression zone.

As mentioned previously, in the slab–column connections subjected to punching failure, a significant amount of flexural cracking is concentrated within the critical section around the column. Thus, the shear strength of the connections is determined at the critical section as per the following equation:

$$V_c = v_c b_0 d = \sqrt{f_{te}(f_{te}+f_{cc})}b_0 c_u \tag{2}$$

where b_0 is the critical perimeter. In the KDS 14 model, b_0 [$=2(c_1+c_2+2d)$] is set at a distance of 0.5 times the slab effective depth from the column faces. This is similar to the specifications in the existing ACI 318, CSA, and JSCE codes, where c_1 and c_2 are the dimensions of the column section.

Prior experimental and theoretical investigations have shown that concrete members subjected to shear exhibit a size effect. This results in a reduction in tensile fracture strength. In addition, the shear stress

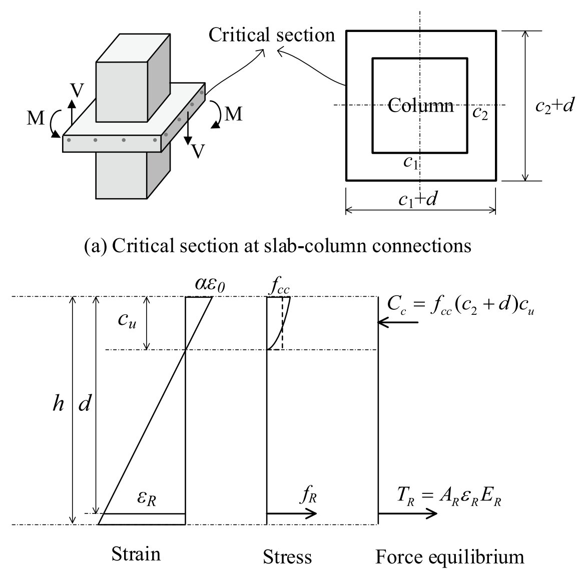

Fig. 3 Force equilibrium and stress–strain compatibility at the critical section

capacity decreases owing to stress concentration at the corners of the rectangular critical section around the column caused by punching failure. To account for these effects, the KDS 14 model adopted the size effect factor, k_s, and aspect ratio factor, k_{b0}, based on the studies by Birkle and Dilger (2008) and Manterola (1966), respectively. Thus, V_c is finally expressed as:

$$V_c = k_s k_{b0} c_u b_0 \sqrt{f_{te}(f_{te}+f_{cc})} \tag{3}$$

where

$$k_s = 0.75 \le \sqrt[4]{300/d} \le 1.1 \tag{4}$$

$$k_{b0} = 4/(\alpha_s b_0 d)^{0.5} \le 1.25 \tag{5}$$

Here, α_s is set to 1, 1.33, and 2 for interior, exterior, and corner connections, respectively.

In Eq. (3), the average compressive normal stress acting on the compression zone, $f_{cc}\left[=(1/c_u)\int_0^{c_u}\sigma_c(z)dz\right]$, can be determined through the integration of the stress distribution over the compression zone depth. Using the parabolic distribution of compressive stress, $\sigma_c(\varepsilon) = f_c'\left[2\left(\frac{\varepsilon}{\varepsilon_0}\right) - \left(\frac{\varepsilon}{\varepsilon_0}\right)^2\right]$ (Vecchio et al., 1986, Matamoros et al., 2003), f_{cc} can be derived as follows:

$$f_{cc} = \left(\alpha - \alpha^2/3\right)f_c' \tag{6}$$

where α is the ratio between the current compressive and compressive normal strains at extreme compression fiber at critical section, ε_0 [≈ 0.002] is the compressive strain corresponding to the concrete compressive strength, and z is the distance from the neutral axis.

By assuming the flat plate as two orthogonal beams with effective widths of ($b_1 = c_1 + d$) and ($b_2 = c_2 + d$) (Choi et al., 2007, 2014), the depth of compression zone in Eq. (3) can be determined based on the force equilibrium and strain compatibility at the critical section, as illustrated in Fig. 3:

$$C_c = T_R, \text{ or} \tag{7a}$$

$$f_{cc}(c_2 + d)c_u = A_R \varepsilon_R E_R = \rho_R (c_2 + d) d \varepsilon_R E_R \tag{7b}$$

$$\varepsilon_R = \alpha \varepsilon_0 (d - c_u)/c_u \tag{8}$$

where C_c is the resultant compressive force of concrete in the compression zone, T_R is the tensile force developed in the tensile reinforcement, A_R and E_R are the total cross-sectional area and elastic modulus of the tensile reinforcement, respectively, ρ_R is the longitudinal reinforcement ratio, and ε_R is the strain in tensile reinforcement.

By substituting Eqs. (6) and (8) into Eq. (7b), the depth of the compression zone can be determined be solving a quadratic equation as follows:

$$f'_c\left(\alpha - \frac{\alpha^2}{3}\right)\left(\frac{c_u}{d}\right)^2 + \alpha\varepsilon_0 E_R \rho_R \frac{c_u}{d} - \alpha\varepsilon_0 E_R \rho_R = 0 \tag{9}$$

The final expression for calculating c_u is obtained by solving Eq. (10):

$$\frac{c_u}{d} = \frac{-\rho_R E_R \alpha\varepsilon_0 + \sqrt{(\alpha\varepsilon_0\rho_R E_R)^2 + 4f'_c\left(\alpha - \frac{\alpha^2}{3}\right)\alpha\varepsilon_0\rho_R E_R}}{2\left(\alpha - \frac{\alpha^2}{3}\right)f'_c} \tag{10}$$

As the term $\left[(\alpha\varepsilon_0\rho_R E_R)^2\right]$ is very small compared to $\left[4f'_c\left(\alpha - \frac{\alpha^2}{3}\right)\alpha\varepsilon_0\rho_R E_R\right]$, it can be neglected. Thus, Eq. (10) is simplified as follows:

$$c_u = d\left[-\frac{\rho_R E_R \alpha\varepsilon_0}{2\left(\alpha - \frac{\alpha^2}{3}\right)f'_c} + \sqrt{\frac{\alpha\varepsilon_0\rho_R E_R}{\left(\alpha - \frac{\alpha^2}{3}\right)f'_c}}\right] \tag{11}$$

3 KDS 14 Model Modification for Punching Shear Strength Evaluation of FRP-RC Slab–Column Connections

The punching shear strength based on the KDS 14 model was originally developed for steel-RC slab–column connections. The average compressive normal stress (f_{cc}) in Eq. (6) and the depth of compression zone (c_u) in Eq. (11), which significantly influence punching shear strength, vary according to the magnitude of strain at the extreme compression fiber ($\alpha\varepsilon_0$) at critical section. In concrete slabs, which are typically designed with low to moderate flexural reinforcement ratios, the punching shear failure at slab–column connections typically occurs immediately before or after the flexural yielding of the steel reinforcement. Cross-sectional analysis (Choi et al., 2014; Dinh et al., 2024a) indicates that the average shear stress capacity reaches its maximum when the compressive strain at the compression fiber reaches or exceeds ε_0 [$=0.002$], consistent with the test observations by Kinnunen and Nylander (1960). Therefore, in the KDS 14 model, the punching shear strength of steel-RC connections is defined at $\varepsilon_0 \approx 0.002$ ($\alpha = 1$). By assuming $\varepsilon_0 \approx 0.002$ for concrete and $E_R = [E_s \approx 200{,}000]$ MPa for steel rebars, the KDS 14 model mathematically simplifies the expressions (6) and (11) for average compressive normal stress (f_{cc}) and the depth of the compression zone (c_u), respectively, as functions of concrete compressive strength (f'_c) and tensile reinforcement ratio (ρ_s), using the following final expressions:

$$f_{cc} = (2/3)f'_c \tag{12}$$

$$c_u = d\left(25\sqrt{\frac{\rho_s}{f'_c}} - 300\frac{\rho_s}{f'_c}\right) \quad , \quad \rho_s \geq 0.005 \tag{13}$$

For evaluating the punching shear strength of slab–column connections reinforced with FRP rebars, Eq. (11) can be effectively utilized to calculate the compression zone depth. Previous studies (Elgabbas et al., 2016; Huang et al., 2020; Nguyen-Minh et al., 2013; Salihi & Hamad, 2023) indicated that the concrete compressive strain at the extreme compression fiber within the critical section in slab–column connections reinforced with FRP rebars was smaller compared to those reinforced with steel rebars. This was primarily owing to the lower stiffness of FRP. However, this strain typically approached the ε_0 value. Therefore, when modifying the KDS 14 model for FRP-RC members, an α value of 1.0 was adopted. This was analogous to the steel-RC counterparts and corresponded to ($f_{cc} = 2/3f'_c$). By assuming $\varepsilon_0 \approx 0.002$ for concrete and using $E_R = E_f$ and $\rho_R = \rho_f$ for FRP rebars, Eq. (11) can thus be redefined in a simplified form as:

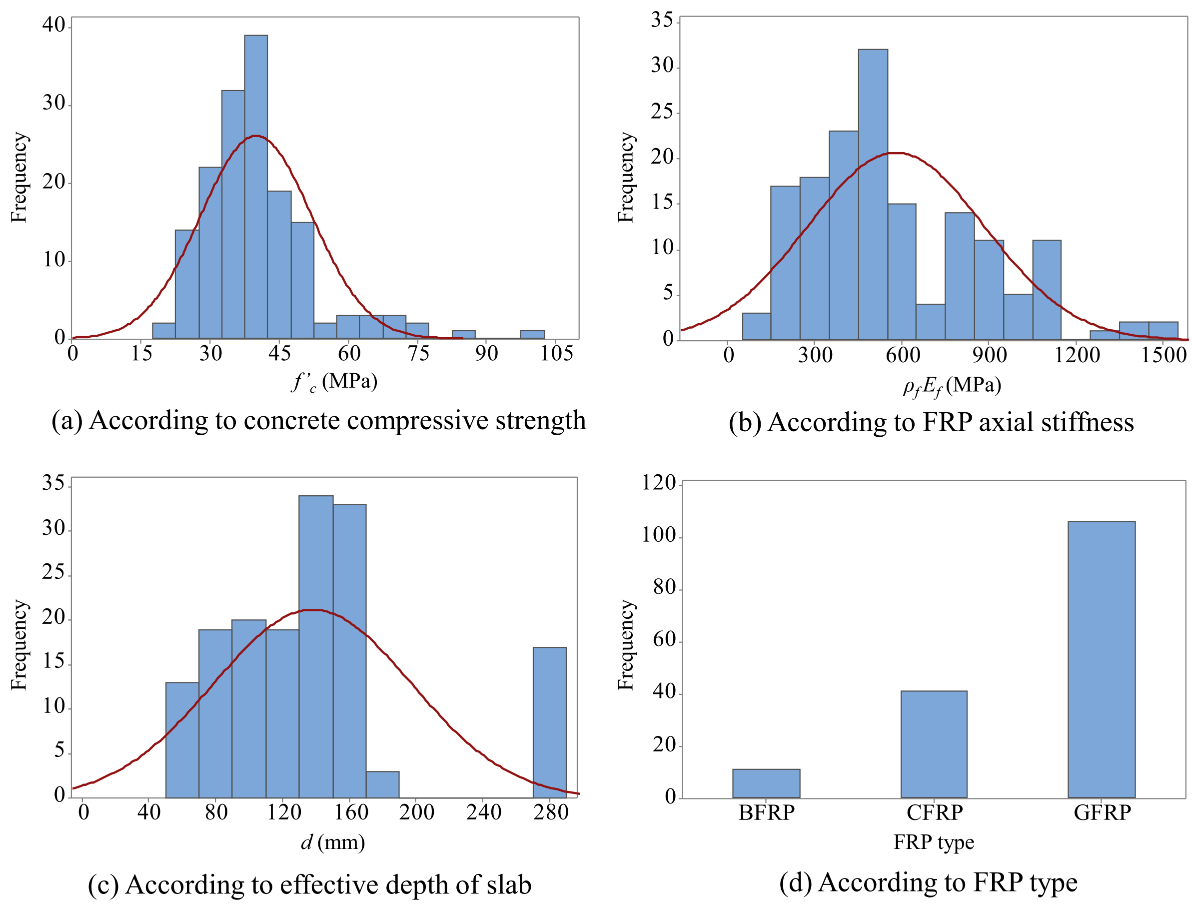

Fig. 4 Distribution of FRP-RC slab–column connections according to various parameters

$$c_u = d\left(\frac{1}{18}\sqrt{\frac{\rho_f E_f}{f_c'}} - \frac{1}{650}\frac{\rho_f E_f}{f_c'}\right) \tag{14}$$

where E_f and ρ_f are the elastic modulus and reinforcement ratio of FRP rebars, respectively. Alternatively, by substituting the quantity $\rho_R E_R$ in Eq. (11) with $\rho_f E_f\left[= \rho_f \frac{E_f}{E_s} E_s = \rho_{s,e} E_s\right]$, an expression similar to that of the KDS 14 model can be derived, which considers the material properties of FRP reinforcement:

$$c_u = d\left(25\sqrt{\frac{\rho_{s,e}}{f_c'}} - 300\frac{\rho_{s,e}}{f_c'}\right) \tag{15}$$

where $\rho_{s,e}\left[= \rho_f E_f / E_s\right]$ is the equivalent longitudinal reinforcement ratio, adjusted for considering the modulus ratio between FRP and steel rebars. The design equations of the modified KDS 14 model are summarized in Table 1.

4 Model Verification and Discussion

4.1 Database of FRC-RC Slab–Column Connections

A comprehensive database of FRP-RC slab–column connections was utilized to verify the applicability of the modified KDS 14 model. The dataset in the Appendix encompassed 150 interior slab–column connection specimens subjected to concentric load. Here, 143 specimens were tested without FRP shear reinforcement (Table A1) and 7 specimens were tested with FRP shear reinforcement (Table A2). Figure 4 illustrates the distribution of specimen numbers in the database according to various test parameters: concrete compressive strength (f'_c) ranging as 21.1–98.3 (MPa), axial stiffness of FRP reinforcement ($\rho_f E_f$) ranging as 99–1530 (MPa), slab effect depth (d) varying as 55–285 (mm), and different types of FRP rebars: carbon FRP (CFRP), glass FRP (GFRP), or basalt FRP (BFRP).

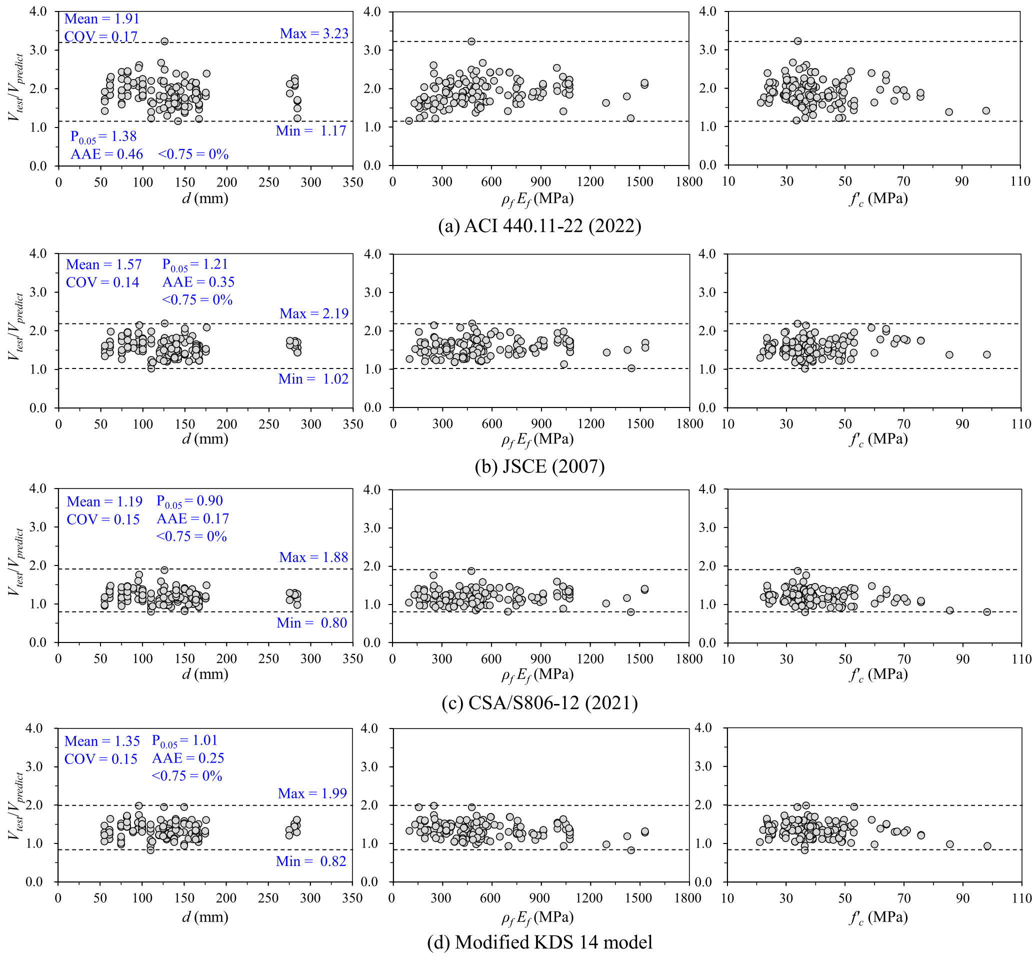

Fig. 5 Comparative analysis of strength ratio for FRP-RC slab–column connections without shear reinforcement using different design equations

4.2 Assessment of Modified KDS 14 Model and Comparison with Existing Design Methods

Tables A1 and A2 in the Appendix summarize the test results for the punching shear strength for two datasets of FRP-RC slab–column connections. One presents the results of those without shear reinforcement and the other with shear reinforcement. Further, the prediction results using the modified KDS 14 model are also presented. Figures 5 and 6 provide a comparative assessment of the modified KDS 14 model against the ACI 440.11-22, JSCE, and CSA/S806-12 provisions. The trends of the strength ratio $V_{test}/V_{predict}$ were examined according to various key design parameters. The minimum, maximum, and average values, as well as the statistical parameters such as the coefficient of variation (COV) and the average absolute error (AAE) are indicated. The AAE is calculated using Eq. (16) as follows:

$$\mathrm{AAE} = \frac{1}{n}\sum_{i=1}^{n}\left|\frac{V_{predict,i} - V_{test,i}}{V_{test,i}}\right| \tag{16}$$

where n is the number of test specimens used in the statistics and $V_{test,i}$ and $V_{predict,i}$ are the test result and prediction, respectively. AAE is a key statistical measure that indicates the correlation between the prediction and test results. The lower the AAE value, the better the model correlates with a dataset.

Furthermore, the safety of different design equations was assessed using the 5% fractile indicator ($P_{0.05}$), assuming a normal distribution of the ratio $V_{test}/V_{predict}$. The $P_{0.05}$ value is generally accepted as a characteristic value of resistance in limit state theory (EN1990:2002, 2002). The closer the 5% fractile value is to one, the better the safety. In addition, the figures present the percentage of specimens with $V_{test}/V_{predict}$ less than 0.75, which corresponded to the strength reduction factor for the shear design.

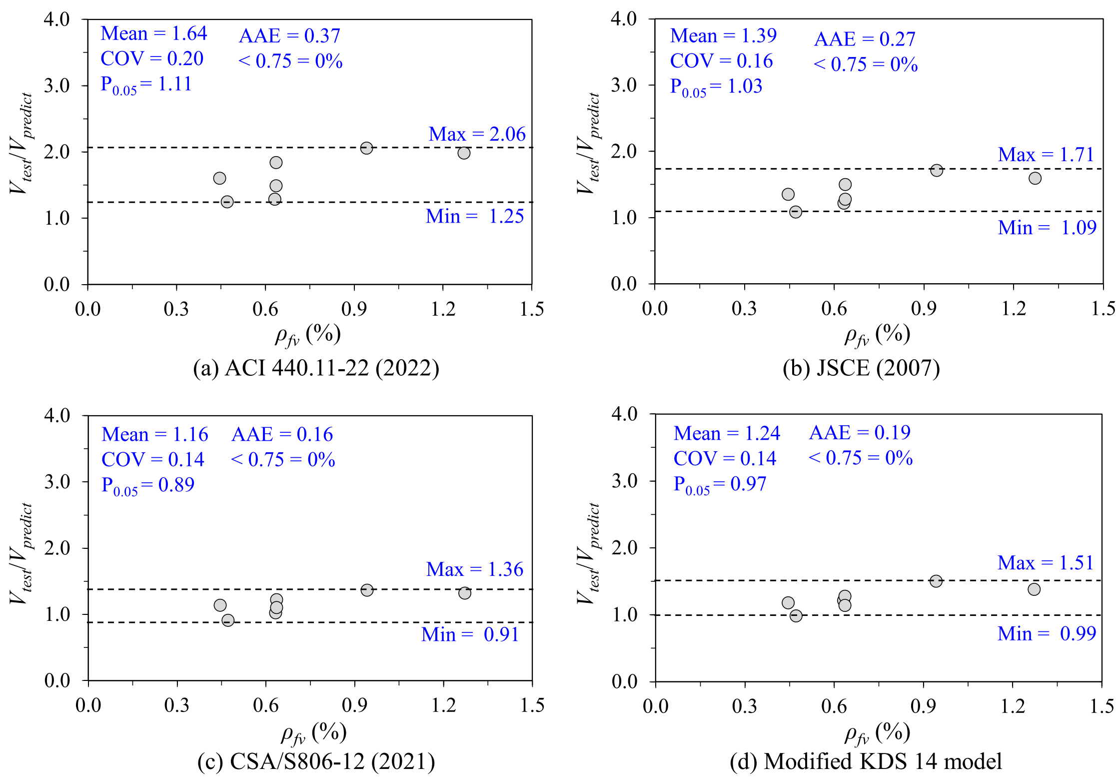

Fig. 6 Comparative analysis of strength ratio for FRP-RC slab–column connections with shear reinforcement

Figure 5 presents the strength ratio $V_{test}/V_{predict}$ for FRP-RC slab–column connections without shear reinforcement as per the slab effective depth, axial stiffness, and concrete compressive strength based on the ACI 440 (Fig. 5a), JSCE (Fig. 5a), CSA codes (Fig. 5c), and modified KDS 14 model (Fig. 5d). Overall, all prediction models were found to demonstrate conservatism when compared to experimental results across various design parameters. ACI 440.11-22 exhibited the highest scattering with a COV of 17% and the highest conservatism compared to test results (mean value of 1.91 and $P_{0.05}$ of 1.38). The modified KDS 14 model exhibited similar scatteredness compared to the JSCE 2007 and CSA models with a COV of approximately 15%. In addition, the modified KDS 14 model showed a good correlation with the dataset, evidenced by an AAE of 0.25 and a mean strength ratio of 1.35. Furthermore, the modified KDS 14 model produced strength ratio values greater than 0.75 and a $P_{0.05}$ value approaching one. Thus, the safety and reliability of the modified KDS 14 model was confirmed.

Figure 6 presents the strength ratio $V_{test}/V_{predict}$ for FRP-RC slab–column connections with FRP shear reinforcement tested by Hassan et al. (2014). It also elucidates the comparative assessment against existing design codes. Most current provisions of FRP design do not account for the contribution of FRP shear reinforcement in shear strength evaluation of two-way slabs. In this study, the punching shear strength, V_n, of FRP-RC slab–column connections with FRP shear reinforcement was evaluated using the design method for two-way shear of steel-RC members:

$$V_n = V_c + V_{sf} \tag{17}$$

$$V_{sf} = \frac{A_{fv} f_{fv} d}{s_{fv}} \tag{18}$$

where V_{sf} is the FRP shear reinforcement contribution to the punching shear capacity, A_{fv} is the total cross-sectional area of the FRP stirrups on a concentric line parallel to the column perimeter, s_{fv} is the FRP stirrup spacing from the column face, and f_{fv} is the effective stress. Further, f_{fv} was determined based on the strain limitation developed in FRP shear reinforcement (for one-way shear) according to ACI 440.11-22 (2022):

$$f_{fv} = 0.005 E_{fv} \leq f_{fb} \tag{19}$$

where E_{fv} and f_{fb} are the elastic modulus and tensile strength of the bent portion of the FRP shear reinforcement, respectively. The strength ratios in Fig. 6 were obtained as per FRP shear reinforcement ratio, ρ_{fv}, at a

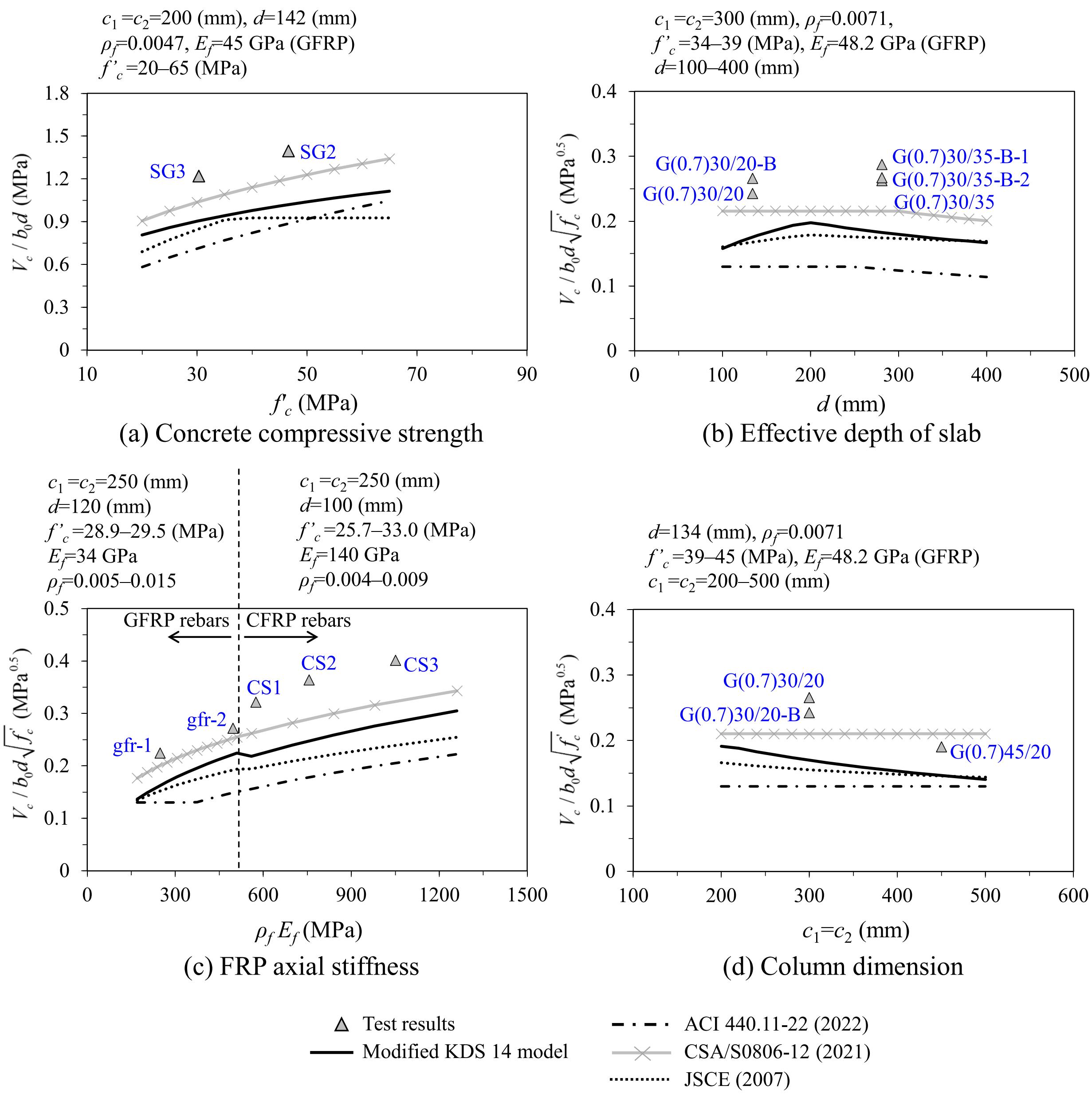

Fig. 7 Parametric study

critical perimeter of 0.5 from the column face. This was determined as follows:

$$\rho_{fv} = \frac{n_s A_{fv}}{s_{fv} b_0} \tag{20}$$

where n_s is the number of FRP stirrups within a critical perimeter.

The prediction results presented in Fig. 6 and Table A2 indicated that the punching shear strength predictions using Eqs. (17)–(20) yielded conservative results and exhibited reasonable correlation with the experimental data across different shear reinforcement ratios of FRP rebars. Both the modified KDS 14 method and existing design codes, when used to calculate V_c in Eq. (15), yielded zero percentage of specimens with $V_{test}/V_{predict}$ ratio of less than 0.75. However, with the same contributions from FRP shear reinforcement calculated using Eq. (18), the overall strength prediction results using the modified KDS 14 model (Fig. 6d) exhibited a better correlation with the test results compared to the existing design codes (Fig. 6a–c). Specifically, the modified KDS 14 model yielded a lower COV of 14%, lower mean value of 1.25, lower AAE index of 0.19, and acceptable $P_{0.05}$ value of 0.97 for safety design. Thus, the results indicated an improvement in the prediction accuracy when using the modified KDS 14 model for calculating V_c, compared to the existing design codes.

5 Parametric Study

Figure 7 presents a parametric study conducted using the modified KDS 14 model and existing design codes. The primary design parameters affecting the punching shear stress capacity $[V_c/b_0 d]$ at the critical section of FRP-RC slab–column connections were investigated. The results were compared with the experimental outcomes from previous studies to assess the reliability of the design models.

Figure 7a presents the results of the investigation of the influence of concrete compressive strength. The analytical specimens were reinforced with GFRP rebars and exhibited concrete compressive strengths ranging as 20–65 MPa. The other design parameters were consistent with specimens SG3 and SG2 tested by El-Ghandour et al. (2003). As evident, all models accounted for the effect of the concrete compressive strength in the design equations. An increase in concrete compressive strength increased the predicted shear stress capacity, which was consistent with the experimental results by El-Ghandour et al. (2003) for specimens SG3 and SG2. In case of the modified KDS 14 model, increased compressive strength enhanced the tensile strength of concrete, thereby increasing the overall shear resistance in the compression zone. It should be noted that in case of the JSCE model, the semiempirical equation considered the effect of tensile strength $\left[f_{pcd} = 0.2\sqrt{f'_c}\right]$, similar to that in case of the KDS 14 model. However, for conservative design, the JSCE model adopted an upper bound limit of 1.2 MPa (refer to Table 1), which yielded a constant shear stress capacity for $f'_c \geq 36$ MPa, as illustrated in Fig. 7a.

Figure 7b presents the results of the investigation of the influence of the effective depth of the slab. The analytical specimens were reinforced with GFRP rebars and had slab effective depths ranging as 100–400 mm. The other design parameters matched those of specimens tested by Hassan et al., (2013a, 2013b). Owing to the variation in the concrete compressive strength of the test specimens, the shear stress capacity was normalized by the square root of the compressive strength ($\sqrt{f'_c}$) to minimize this effect. Figure 7b and Table A1 indicate that, despite an increase in slab effective depth increasing the punching shear strength, the shear stress capacity at the critical section varied insignificantly for slender members like slab–column connections. This trend was consistent with the experimental results by Hassan et al., (2013a, 2013b) for different specimens. For the modified KDS 14 and JSCE models, an upper limit of normalized shear stress capacity was observed with variations in effective depth. This value results from incorporating the size effect factor and aspect ratio factor of the critical section in the design equations (see Table 1). It should be noted that most existing FRP design codes consider the size effect factor in the design equations based on the calibration of the steel–RC members (Table 1). Thus they typically exhibit a slight reduction in shear stress capacity for large slab thickness, particularly exceeding 300 mm (Fig. 7b). However, the majority of test specimens in the current database had slab thicknesses of less than 280 mm. Therefore, further investigations are required to improve the size effect factor for FRP-RC design codes.

Figure 7c illustrates the influence of the FRP axial stiffness ($\rho_f E_f$) on the normalized shear stress capacity of slab-column connections. The first group, based on a study by Ospina et al. (2003), included specimens reinforced with GFRP rebars with E_f= 34 GPa and ρ_f varying within 0.5–1.5%. The second group, based on a study of Zhang et al. (2005), included specimens reinforced with CFRP rebars with E_f= 140 GPa and ρ_f varying within 0.4–0.9%. Figure 7c indicated an apparent trend where for each group with the same FRP reinforcement type, increasing FRP axial stiffness by increasing the reinforcement ratio, increased the predicted shear stress capacity. This was consistent with the experimental results by Ospina et al. (2003) and Zhang et al. (2005).

Further, when comparing the two groups of specimens with insignificant variation in design parameters (the same column dimensions, d varying as 100–120 mm, f'_c varying as 25–33 MPa, and ρ_f varying within 0.5–1.5%), the use of CFRP rebars with elastic modulus approximately four times higher than that of GFRP rebars increased the overall FRP axial stiffness. This resulted in a significant improvement in the shear stress capacity of specimens CS1, CS2, and CS3 compared to specimens gfr-1 and gfr-2. Overall, all the existing codes exhibited a consistent trend with the experimental results by incorporating the quantity ($\rho_f E_f$) in the semiempirical design equations. For the modified KDS 14 model, which was based on compression zone failure theory, as described in Eq. (14), the increase in FRP axial stiffness increased the compression zone depth (c_u) owing to the conditions of force equilibrium and strain compatibility, thereby increasing the overall punching shear strength of the connection.

Figure 7d illustrates the influence of the column dimensions on the normalized shear stress capacity of slab–column connections. The analytical specimens were reinforced with GFRP rebars and had square column dimensions ranging as 200–500 mm. The other design parameters were consistent with those of specimens tested by Hassan et al. (2013a). The results of the parametric analysis indicated that, while the ACI 440 and CSA models do not consider the effect of column dimensions, both the modified KDS 14 and existing JSCE models exhibited a reduction in shear stress capacity at the critical section with increase in the column dimensions. This was owing to the incorporation of an aspect ratio factor in the design equations (Sect. 2). This trend was consistent with the experimental results reported by Hassan et al. (2013a).

6 Conclusions

This study evaluated the applicability of the KDS 14 design method for the punching shear strength prediction of slab–column connections reinforced with FRP rebars. The KDS 14 model was modified by revising the equation used for determining the depth of the compression zone (c_u), taking into account the material properties of FRP reinforcement. To assess the reliability of the modified model, a comparative analysis was conducted using the modified KDS 14 model and existing state-of-the-art design codes over a comprehensive database comprising 150 FRP-RC slab–column specimens with and without shear reinforcement collected from previous studies. The primary conclusions drawn from this study are as follows.

1. The modified KDS 14 model exhibited promising performance in terms of predicting the punching shear strength of a large dataset of FRP-RC slab–column connections without shear reinforcement. The model demonstrated scatter similar to that of the JSCE 2007 and CSA models, with a COV of approximately 15%. Further, it exhibited better correlation with the dataset compared to existing design codes, as indicated by a lower AAE index of 0.25 and a lower mean strength ratio of 1.35. In addition, the modified KDS 14 model produced strength ratio values greater than 0.75 and a $P_{0.05}$ value approaching one, thereby indicating the acceptable conservatism in the design.
2. When predicting the punching shear strength of FRP-RC slab–column connections with shear reinforcement, the modified KDS 14 model exhibited a reasonable and conservative correlation with the experimental data, with zero percentage of specimens having strength ratios of less than 0.75. Further, the modified KDS 14 model exhibited a better correlation with the test results compared to most existing design codes, with a lower COV of 14%, lower mean value of 1.24, and lower AAE of 0.19.
3. A parametric study was conducted to examine the primary design parameters that affected the punching shear stress capacity at the critical section of FRP-RC slab–column connections using the modified KDS 14 model and existing design codes. Overall, all prediction models exhibited similar trends consistent with the experimental results as per variations in design parameters (e.g., concrete compressive strength, slab effective depth, FRP axial stiffness, and column dimensions).
4. In case of the modified KDS 14 model, which was based on the compression zone failure theory, an increase in compressive strength enhanced the tensile strength of the concrete, thereby contributing to the overall shear resistance in the compression zone. A similar trend was observed with an increase in FRP axial stiffness, which increased the punching shear stress capacity owing to the increased depth of the compression zone caused by force equilibrium and strain compatibility conditions. In addition, an increase in the slab effective depth within the investigated range resulted in insignificant variation in the predicted punching shear stress capacity at the critical section. Furthermore, by incorporating an aspect ratio factor in the design equations, the modified KDS 14 model demonstrated a trend consistent with the experimental results. It exhibited a reduction in shear stress capacity at the critical section with increase in the column dimensions.

Supplementary Information

The online version contains supplementary material available at https://doi.org/10.1186/s40069-024-00754-0.

Additional file 1.

Acknowledgements

The authors gratefully acknowledge the financial support provided by the Basic Science Research Program through the National Research Foundation of Korea funded by the Ministry of Education (NRF-2022R1A2C2004351), and by Grant (RS-2022-00143493) from Digital-Based Building Construction and Safety Supervision Technology Research Program funded by Ministry of Land, Infrastructure and Transport of Korean Government.

Author Contributions

N.H.D: conceptualization, methodology, data curation, writing—original draft. S.-H. K: data curation, investigation. K.-K. C: conceptualization, writing—original draft, review and editing, funding acquisition. All authors read and approved the final manuscript.

Availability of Data and Materials

The authors declare that the datasets used or analyzed during the current study are available from the corresponding author on reasonable request.

Declarations

Ethics Approval and Consent to Participate
Not applicable.

Consent for Publication
Not applicable.

Competing Interests
The authors declare that there are no competing interests.

Received: 29 August 2024 Accepted: 11 December 2024
Published online: 06 March 2025

References

ACI Committee, and International Organization for Standardization, ACI 318-14: Building code requirements for structural concrete and commentary. American Concrete Institute, 2014.
ACI Committee 440. Guide for the design and construction of structural concrete reinforced with fiber-reinforced polymer (FRP) Bars. ACI 440.1R-15. Farmington Hills: American Concrete Institute; 2015.
ACI Committee 440. Building code requirements for structural concrete reinforced with glass fiber-reinforced polymer (GFRP) bars—Code and commentary. ACI 440.11-22. Farmington Hills: American Concrete Institute; 2022.
Almomani, Y., Alawadi, R., Tarawneh, A., Alghossoon, A., & Aldiabat, A. (2024). Punching shear of FRP-RC slab–column connections: A comprehensive database. *Journal of Composites Science, 8*(4), 145.
Birkle, G., & Dilger, W. H. (2008). Influence of slab thickness on punching shear strength. *ACI Structural Journal, 105*(2), 180.
Canadian Standard Association (CAN/CSA S806-12). Design and construction of building structures with fibre-reinforced polymers. Canadian Highway Bridge Design Code, Rexdale, Ontario, 2021.
CEN. (2002). EN1990: Eurocode - Basis of structural design, European Commission, Brussels, Belgium.
Choi, K.-K., & Park, H. G. (2010). Shear strength model for interior flat plate-column connections. *Journal of the Korea Concrete Institute, 22*(3), 345–356.
Choi, K.-K., Shin, D. W., & Park, H. G. (2014). Shear-strength model for slab-column connections subjected to unbalanced moment. *ACI Structural Journal*, *111*(3).
Choi, K.-K., Taha, M. M. R., Park, H. G., & Maji, A. K. (2007). Punching shear strength of interior concrete slab–column connections reinforced with steel fibers. *Cement and Concrete Composites, 29*(5), 409–420.
Dinh, N. H., Noh, J., Choi, K. K., & Park, H. G. (2024a). Punching shear strength of isolated concrete column footings with low shear span-depth ratios. *ACI Structural Journal*, *121*(3).
Dinh, N. H., Kim, S. H., & Choi, K. K. (2024a). Simplification of KDS 14 design method for slab-column connections subjected to unbalanced moment. *International Journal of Concrete Structures and Materials, 18*(1), 72.
Dinh, N. H., Roh, Y. S., & Truong, G. T. (2024c). Shear strength model of FRP-reinforced concrete beams without shear reinforcement. *Structures* (Vol. 64, p. 106520). Elsevier.
Dulude, C., Hassan, M., Ahmed, E. A., & Benmokrane, B. (2013). Punching shear behavior of flat slabs reinforced with glass fiber-reinforced polymer bars. *ACI Structural Journal, 110*(5), 723.
Elgabbas, F., Ahmed, E. A., & Benmokrane, B. (2016). Experimental testing of concrete bridge-deck slabs reinforced with basalt-FRP reinforcing bars under concentrated loads. *Journal of Bridge Engineering, 21*(7), 04016029.
El-Ghandour, A. W., Pilakoutas, K., & Waldron, P. (2003). Punching shear behavior of fiber reinforced polymers reinforced concrete flat slabs: Experimental study. *Journal of Composites for Construction, 7*(3), 258–265.
Hassan, M., Ahmed, E. A., & Benmokrane, B. (2013a). Punching shear strength of glass fiber-reinforced polymer reinforced concrete flat slabs. *Canadian Journal of Civil Engineering, 40*(10), 951–960.
Hassan, M., Ahmed, E., & Benmokrane, B. (2013b). Punching-shear strength of normal and high-strength two-way concrete slabs reinforced with GFRP bars. *Journal of Composites for Construction, 17*(6), 04013003.
Hassan, M., Ahmed, E. A., & Benmokrane, B. (2014). Punching-shear design equation for two-way concrete slabs reinforced with FRP bars and stirrups. *Construction and Building Materials, 66*, 522–532.
Huang, Z., Zhao, Y., Zhang, J., & Wu, Y. (2020). Punching shear behaviour of concrete slabs reinforced with CFRP grids. *Structures, 26*, 617–625.
Japan Society of Civil Engineers (JSCE). Recommendation for design and construction of concrete structures using continuous fiber reinforcing materials, concrete engineering series no. 23, JSCE: Tokyo, Japan, 2007.
Kinnunen, S., & Nylander, H. S. E. (1960). Punching of concrete slabs without shear reinforcement. *(No Title)*.
Korea Concrete Institute (KCI), Design code for shear and torsion of concrete structures (KDS 14 20 22), Korea Design Standard (KDS), Ministry of Land, Infrastructure, and Transport of Korea, Seoul, Republic of Korea; 2021. (in Korean).
Lee, J. H., Yoon, Y. S., Cook, W. D., & Mitchell, D. (2009). Improving punching shear behavior of glass fiber-reinforced polymer reinforced slabs. *ACI Structural Journal, 106*(4), 427.
Manterola, M. (1966). Poinçonnement de dalles sans armature d'effort tranchant. *Comité EuroPéEN du Béton: Dalles, Structures Planes, CEB-Bull d'Information*, (58).
Matamoros, A. B., & Sozen, M. A. (2003). Drift limits of high-strength concrete columns subjected to load reversals. *Journal of Structural Engineering, 129*(3), 297–313.
Matthys, S., & Taerwe, L. (2000). Concrete slabs reinforced with FRP grids. II: Punching resistance. *Journal of Composites for Construction, 4*(3), 154–161.
Mohamed, O. A., & Khattab, R. (2017). Review of punching shear behaviour of flat slabs reinforced with FRP bars. In *IOP Conference Series: Materials Science and Engineering* (Vol. 245, No. 3, p. 032064). IOP Publishing.
Nguyen-Minh, L., & Rovňák, M. (2013). Punching shear resistance of interior GFRP reinforced slab-column connections. *Journal of Composites for Construction, 17*(1), 2–13.
Ospina, C. E., Alexander, S. D., & Cheng, J. R. (2003). Punching of two-way concrete slabs with fiber-reinforced polymer reinforcing bars or grids. *Structural Journal, 100*(5), 589–598.
Pavlović, A., Donchev, T., Petkova, D., & Staletović, N. (2022). Sustainability of alternative reinforcement for concrete structures: Life cycle assessment of basalt FRP bars. *Construction and Building Materials, 334*, 127424.
Peng, F., Xue, W., & Xue, W. (2020). Database evaluation of shear strength of slender fiber-reinforced polymer-reinforced concrete members. *ACI Structural Journal, 117*(3), 273–281.
Ray, B. C., & Rathore, D. (2015). Environmental damage and degradation of FRP composites: A review report. *Polymer Composites*, *36*(3).
Salihi, B., & Hamad, F. (2023). Two-way slab punching shear resistance: Experimental insights into basalt-FRP bar as flexural reinforcement. *Sustainability, 15*(21), 15417.
Schmidt, P., Kueres, D., & Hegger, J. (2020) Contribution of concrete and shear reinforcement to the punching shear resistance of flat slabs. *Engineering Structures 203*, 109872. https://doi.org/10.1016/j.engstruct.2019.109872
Vecchio, F. J., & Collins, M. P. (1986). The modified compression-field theory for reinforced concrete elements subjected to shear. *ACI Journal, 83*(2), 219–231.
Watari, T., Cao, Z., Hata, S., & Nansai, K. (2022). Efficient use of cement and concrete to reduce reliance on supply-side technologies for net-zero emissions. *Nature Communications, 13*(1), 4158.
Zhang, Q., Marzouk, H., & Hussein, A. (2005). A preliminary study of high-strength concrete two-way slabs reinforced with GFRP bars. In *Proceedings of the 33rd CSCE Annual Conference: General Conference and International History Symposium,* Toronto, ON, Canada (pp. 1–10).

Publisher's Note

Ngoc Hieu Dinh is working as a postdoctoral fellow at the Soongsil University, Korea. He received his MS and PhD in architectural engineering from the Soongsil University. His research interests include the seismic design of RC structures and application of fiber reinforced concrete/textile reinforced concrete.

Si-Hyun Kim is a Masters student in the Department of architecture at the Soongsil University, Korea. He received his BE from the School of Architecture, Soongsil University. His research interests include the design and testing of RC structures.

Kyoung-Kyu Choi is a Professor of architectural engineering at the Soongsil University, Korea. He received his BE, MS, and PhD in architectural engineering from the Seoul National University. He was an associate member of Joint ACI–ASCE Committee 445. He has received the ACI Chester Paul Siess Award for Excellence in Structural Research in 2009 and 2012. His research interests include the shear and seismic design of RC structures and application of fiber reinforced concrete.